lubricants

MDPI

Article

Dynamic Performance Analysis of Cage in Four-Point Contact Ball Bearing

Yeteng Li [1], Wenchao Li [1,2], Yongsheng Zhu [1,*], Gaobo He [1], Shuaijun Ma [1] and Jun Hong [1]

[1] Key Laboratory of Education Ministry for Modern Design & Rotor-Bearing System, Xi'an Jiaotong University, Xi'an 710049, China; liyeteng@stu.xjtu.edu.cn (Y.L.); zys_liwenchao@163.com (W.L.); gaobohe@stu.xjtu.edu.cn (G.H.); msj821@stu.xjtu.edu.cn (S.M.); jhong@mail.xjtu.edu.cn (J.H.)
[2] Luoyang Bearing Research Institute Co., Ltd., Luoyang 471039, China
* Correspondence: yszhu@mail.xjtu.edu.cn; Tel.: +86-13991149360

Abstract: Due to the special structure of double-half inner rings, four-point contact ball bearings are prone to uneven forces in the inner raceway during movement, which affects the dynamic performance of the rolling element and cage, and even leads to cage sliding. Dynamic performance of the cage is an important factor affecting the working stability of bearings. In this paper, in order to grasp the operation law of the cage so as to guide the application of four-point contact ball bearings, the dynamic model of four-point contact ball bearings is established by the secondary development of Automatic Dynamic Analysis of Mechanical Systems (ADAMS). The dynamic performance of the cage is analyzed and evaluated with the indexes of vortex radius ratio and vortex velocity deviation ratio of the cage centroid trajectory. The results show the following: the cage stability increases and then decreases to a certain degree with rotating speed-rise; it increases and then decreases with the increase in the pure axial load; under a combination of axial and radial load, the cage moves more smoothly with smaller radial force. Rotating speed has little effect on cage stability, while radial force has a great influence on cage stability, followed by axial load. In order to verify the simulation results, a test bench for rolling bearing cages is developed, and the accuracy of the simulation results is verified by the test results.

Keywords: load distribution; four-point contact ball bearing; bearing dynamics; cage motions experiment

Citation: Li, Y.; Li, W.; Zhu, Y.; He, G.; Ma, S.; Hong, J. Dynamic Performance Analysis of Cage in Four-Point Contact Ball Bearing. *Lubricants* **2022**, *10*, 149. https://doi.org/10.3390/lubricants10070149

Received: 14 April 2022
Accepted: 29 June 2022
Published: 11 July 2022

1. Introduction

As an important part of the high-speed railways, the bogie plays a role in connecting the body and the track, thus its motion stability affects the safety and comfort of the train [1,2]. Figure 1 shows a bogie. The four-point contact ball bearing (FPCBB) is one of the important components of the bogie, which could support axial loads in both directions due to its double-half structure. It is usually used in conjunction with cylindrical roller bearings for locating and supporting. Compared to a traditional paired configuration angular contact ball bearing, FCPBB requires less coaxiality and space between bore and shaft. However, in the motion process, the force between the rolling elements and the double-half raceway will change, inevitably making a four-point contact, three-point contact or two-point contact inside the bearing, which may lead to cage instability. In case of serious instability, it will even cause abnormal heat generation and the early failure of the bearing. Therefore, investigation of its dynamic characteristics is desired.

Research on FPCBB focuses more on wind turbines, aero-engines and robots joints, and most of them are static analysis. For example, Zhang [3] has analyzed the influence of radial load and overturning moment on the load distribution of FPCBB; Li [4] has analyzed the influence of positive and negative clearance on the load distribution of FPCBB; Li and Tang [5] have studied the influence of different parameters on the load–displacement relationship theoretically by establishing the geometric coordination equation of FPCBB.

In the research on the dynamic characteristics of FPCBB, researchers mostly pay more attention to the wind turbine bearings that mainly bear radial load and overturning torque, as well as the thin-walled FPCBB of industrial robots that prefer structural optimization and lightweight design. Wu [6] has analyzed the influence of different speed and preload on the dynamic characteristics of FPCBB of wind turbine generator; Shi [7] has studied the influence of different structural parameters on the dynamic characteristics of four point contact ball bearing under the combined action of axial load and overturning moment; Yang [8] has studied the precise elliptical contact area shape and contact state of thin-walled FPCBB based on the finite element method; Liu [9] has explored the optimization of structural parameters of thin-walled FPCBB from the aspects of contact force between ball and cage and its influence on axial vibration intensity of cage centroid by multi-body dynamics and Hertz contact theory. These studies provide great help for improving the service performance and the efficiency of bearing design.

Figure 1. The bogie of high-speed railway train.

In terms of dynamic analysis of bearings, the establishment of motion differential equations was started by Walters [10]. His model with a 4 degrees of freedom (4-DOF) ball and a 6-DOF cage laid the foundation for dynamic analysis of ball bearing. Based on the study of Walters, Gupta [11–13] studied the complex motion and contact state between the rollers and raceway, and comprehensively analyzed the steady and transient dynamic characteristics of the bearing. Hagiu [14] programmed the calculation of the interaction between bearing components, but the model did not take into account the lubrication. Wijnant [15] constructed the ball bearing dynamic model of considering lubrication film, but the calculation accuracy is dependent on the step size and is difficult to guarantee. Weinzapel [16] established a flexible cage and obtained the rigid–flexible coupling model in order to be closer to the actual working conditions, which makes the calculation more complex. In addition, some scholars [17–20] applied the finite element method to analyze contact characteristics of FPCBB, but due to the complex meshing, these studies are mostly limited to the analysis of large bearings under steady low speed conditions.

Furthermore, some researchers used the commercial software of multi-body dynamics to numerically analyze dynamic characteristics of bearings. For example, Ji [21] used ADAMS to analyze the dynamic characteristics of the instantaneous response of the cage, and studied cage centroid trajectory characteristics under different rotating speeds, loads, radial clearances and the number of steel balls. Hong [22] and Chan [23] also used ADAMS to establish the bearing dynamic model, so as to carry out corresponding researches. Hou [24] built a rigid–flexible hybrid dynamic model of the bearing based on ANSYS and ADAMS, and obtained the motion law of rigid components and the influence of vibration. However, there are relatively few analyses on the dynamic performance for bogie four-point contact ball bearings, a load condition in which axial load is dominant and radial load

is supplementary. Wu [6] analyzed the bearing dynamic feature under main radial load. However, it did not put forward the corresponding evaluation index, and only analyzed the motion characteristics of the bearings under different working conditions. Zhang [25] analyzed the influence of cage structure shape on bearing dynamic characteristics under combined loads by ADAMS. Based on Hertz contact theory, Zhao [26] used ADAMS to establish a bearing dynamic model considering gear meshing, axial load, speed and overturning torque on bearing vibration and contact force.

As mentioned above, no clear evaluation indicators were given for the motion stability analysis of four-point contact ball bearings. The common method for bearing dynamic analysis is based on the multi-body dynamics commercial software, which is greatly affected by the limitation of the software itself and can only consider limited factors. In order to discuss the operation stability of bearings, a general methodology for dynamic performance analysis of cage will be proposed in this work. A dynamic model of FPCBB will be established based on ADAMS secondary development, and the cage centroid trajectory will be discussed under the conditions of radial load and axial load in the following sections. The variation of cage motion stability is described by vortex velocity deviation ratio and vortex radius ratio, the latter referring to the ratio of the difference between the maximum and minimum vortex radius to the average vortex radius. Finally, a test bench will be developed to collect the real speed and cage motion trajectory at different rotating speeds and load conditions to validate the simulation results.

2. Bearing Dynamic Model

2.1. Solid Model Creation

The bearing model is QJ215, which is generally used in the high-speed railway bogie. The structure is shown in Figure 2. The bearing inner rings, outer ring and rolling elements are made of bearing steel, and the cage is made of brass. Specific size and material parameters are shown in Table 1. In this paper, the parametric design method is used to model the FPCBB in ADAMS/View by macro commands and CMD program [27,28]. The 3D model, as shown in Figure 3, can be obtained by inputting corresponding structural parameters.

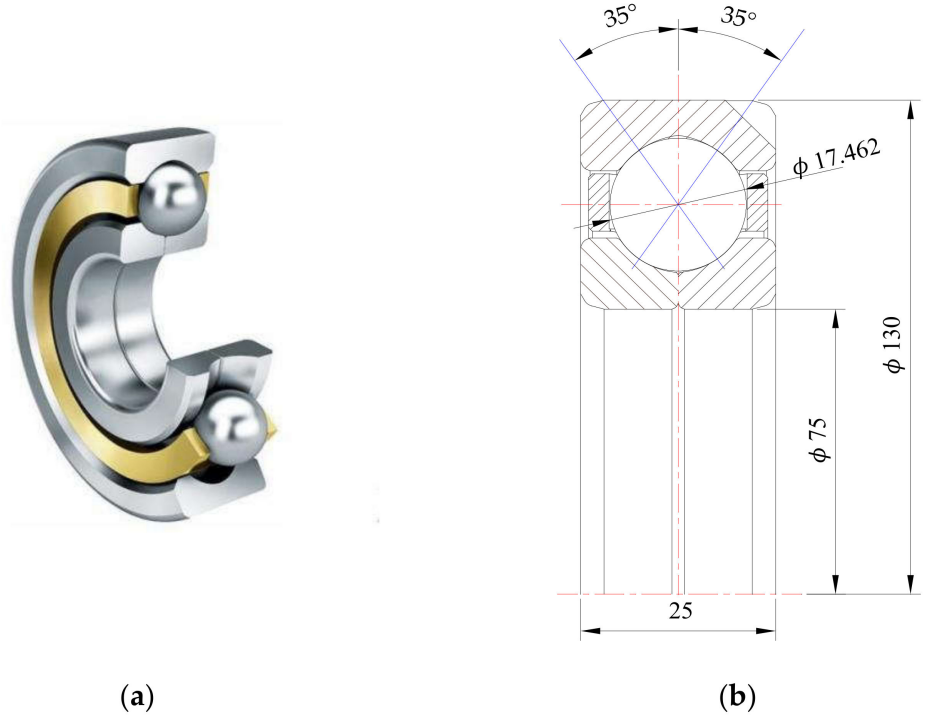

Figure 2. The structure of QJ215. (**a**) A physical picture of QJ215; (**b**) A dimension drawing of QJ215.

Table 1. Dimensional parameters and material parameters of the four-point contact ball bearing.

Characters	Parameter Name	Numerical Value
d	Diameter of inner ring	75 mm
D	Diameter of outer ring	130 mm
D_w	Diameter of ball	17.462 mm
Z	Number of balls	15
B	Width of bearing	25 mm
α	Contact angle	35°
Pd	Radial clearance	27 μm
ΔD_c	Lead gap	20
E_1	Elastic modulus of bearing steel	2.1×10^{11} N/mm^2
ν_1	Poisson ratio of bearing steel	0.29
ρ_1	Density of bearing steel	7.81×10^{-6} kg/mm^3
E_2	Elastic modulus of brass	1.06×10^{11} N/mm^2
ν_2	Poisson ratio of brass	0.324
ρ_2	Density of brass	9.5×10^{-7} kg/mm^3

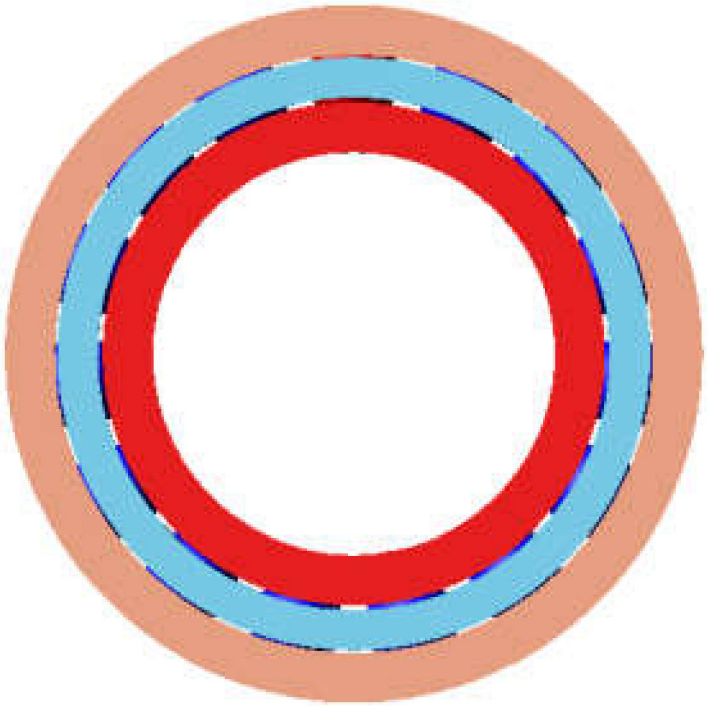

Figure 3. 3D model of QJ215.

2.2. Bearing Dynamics Model Construction Based on GFOSUB

The contact force between bearing components is greatly affected by the recognition accuracy of ADAMS solver on the solid model, and the results are prone to problems such as large values and burrs [29]. For more realistic results, the bearing contact force can be solved directly by GFOSUB subroutine, which can bypass the contact stiffness and ADAMS solver, reducing the negative effects of contact stiffness and other parameters. The process of building a bearing dynamics model based on Gforce Subroutine (GFOSUB) is shown in Figure 4.

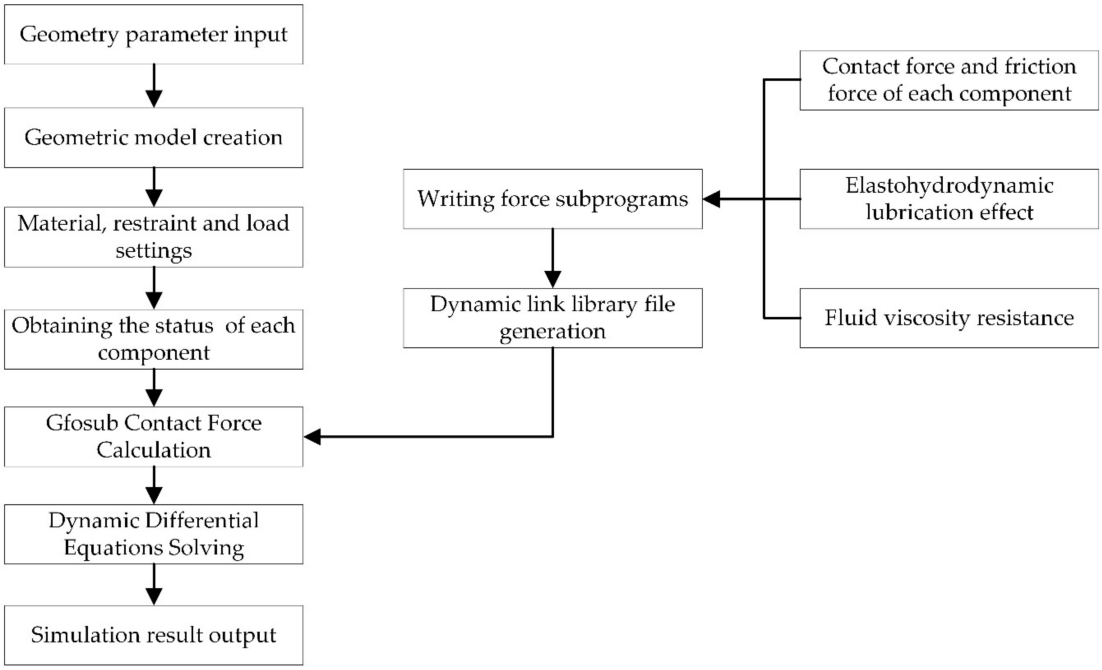

Figure 4. The process of building the bearing dynamics model based on GFOSUB.

Firstly, the geometric model of FPCBB is established by structural parameters, and boundary conditions such as materials, constraints and loads are set to obtain the state information of bearing components, including displacement, speed and acceleration, etc. Meanwhile, the GFOSUB bypasses the Adams contact solver to complete the calculation of force, finally the output results are solved by the differential equation solver. The command box of GFOSUB is shown in Figure 5. The parameters in the red box are ball diameter, groove curvature radius of outer raceway, outer raceway groove bottom diameter, inner raceway groove bottom diameter, dynamic friction coefficient, static friction coefficient, outer ring outer diameter, mass marker point of the inner ring center and mass marker point of the outer ring center. The yellow box is the name of the .dll file where GFOSUB is located. GFOSUB can be called by entering the corresponding parameters.

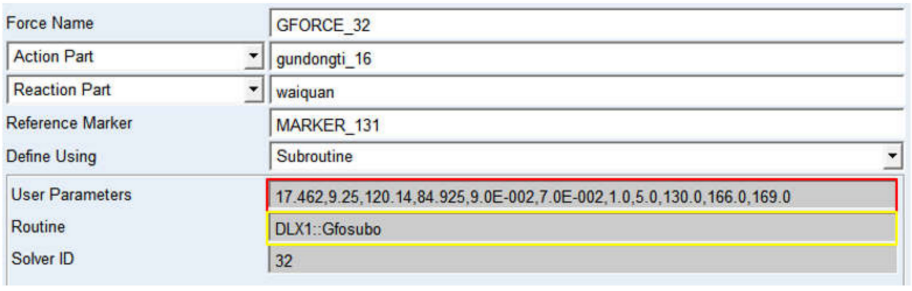

Figure 5. The command box of GFOSUB.

2.3. Boundary Condition Settings

Boundary condition settings mainly include adding freedom constraint, load, driving speed, contact force, etc.

1. Addition of freedom constraints;

In the unconstrained state, the bearing has six degrees of freedom for translation and rotation in X, Y and Z directions. In the actual working process, the outer ring is in a fixed state with 0 degrees of freedom, so it is necessary to add the corresponding restraint sub to restrain its motion. The inner ring has 4 degrees of freedom, i.e., translational movement

in X, Y and Z directions and axial rotation: δ_x, δ_y, δ_z and θ_y; the rolling elements and the cage retain 6 degrees of freedom: δ_x, δ_y, δ_z, θ_x, θ_y and θ_z. The above freedom relationship is shown in Figure 6.

2. Addition of load and driving speed;

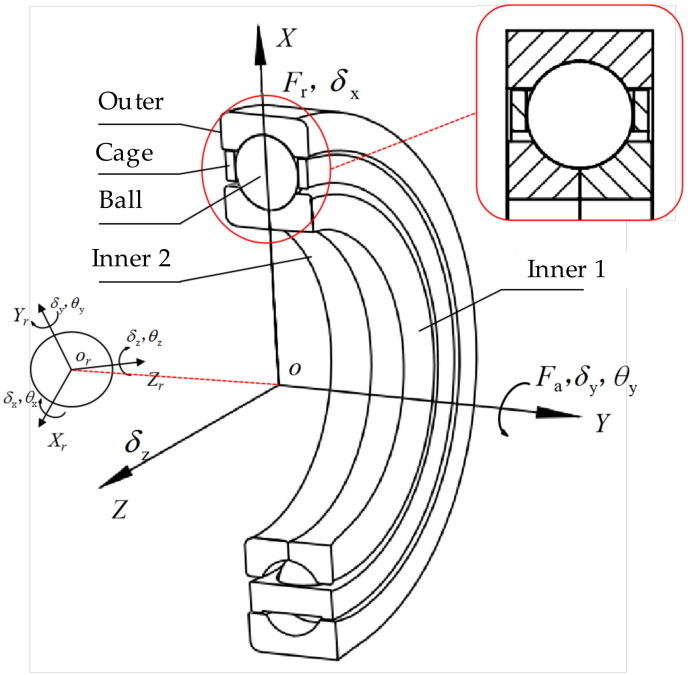

Figure 6. The dynamic model of FPCBB.

For the FPCBB model, it is only subjected to axial and radial loads in the working process, and the load acts on the center of the inner ring. In Figure 6, *F*a is the axial load, *F*r is the radial load. In addition, the driving speed is set in the direction of the axial rotation of the inner ring, and according to the design requirements, the rated speed of the bearing is 5988 r/min.

3. Addition of contact force.

The interaction between the components of the bearing is mainly transmitted according to the contact force. FPCBB has a wide range of contact elements; according to the contact elements, they can be divided into rolling elements and inner rings, rolling elements and outer rings, rolling elements and cages, cages and guide rings, etc. When using ADAMS for dynamic simulation, the contact parameters between the two elements mainly include stiffness, damping and related friction coefficient.

For the FPCBB, the contact model between the rolling elements and the inner and outer rings is point contact, and the bearing contact stiffness K_j (j = i,o) can be calculated by empirical formula [30], such as Equation (1):

$$K_j = 2.15 \times 10^5 \left(\sum \rho\right)^{-1/2} (n_\delta)^{-3/2} \tag{1}$$

where $\sum \rho$ is the curvature of the contact point, and n_δ is the contact deformation coefficient of elastomer.

The calculation of $\sum \rho_i$ and $\sum \rho_o$ is as follows:

$$\sum \rho_i = \frac{4}{D_w} + \frac{2}{d_m - D_w} - \frac{1}{r_i} \tag{2}$$

$$\sum \rho_o = \frac{4}{D_w} - \frac{2}{d_m - D_w} - \frac{1}{r_o} \tag{3}$$

where d_m is the equivalent diameter of bearing, which can be calculated by Equation (4):

$$d_m = (d + D)/2 \tag{4}$$

Replace the bearing parameters to obtain the value of K_j: $K_i = 1.25 \times 10^6$, $K_o = 1.1 \times 10^6$.

In ADAMS, the bearing contact damping is taken as 0.1~0.01% times the contact stiffness and the friction coefficient is about 0.1 [31].

At this point, the dynamics model of FPCBB is completed in ADAMS.

3. Verification of FPCBB Model

For the created bearing model, it is necessary to verify its accuracy to improve the reliability of the simulation results. In this paper, the correctness of the dynamics model is judged by the theoretical calculation results as well as the bearing load distribution curve under the static simulation and dynamics simulation.

Based on the above-mentioned parametric model, an axial load of 2000 N, a radial load of 500 N and a rotating angular speed of 1000 rpm are applied to the center of inner rings. The dynamic simulation of the bearing is implemented in ADAMS software, the velocities and dynamic contact forces of the bearing are shown in Figure 7.

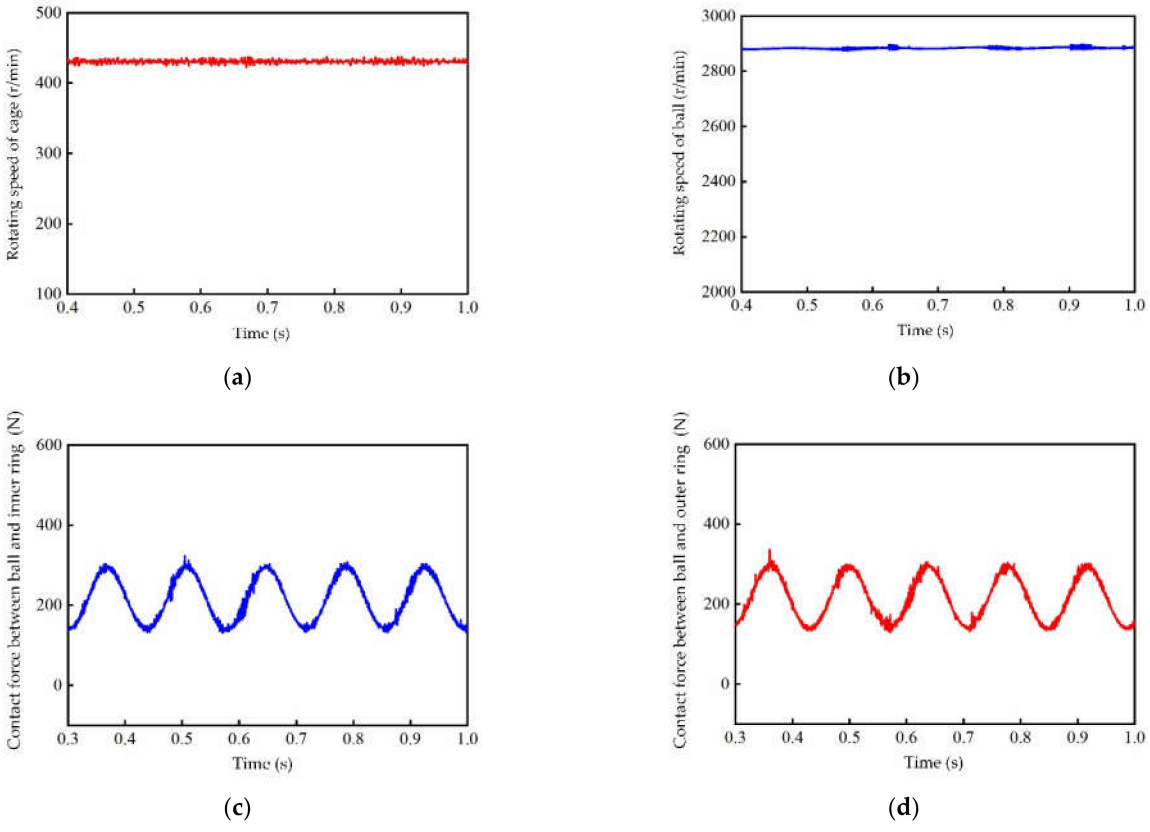

Figure 7. Velocities and dynamic contact forces of QJ215. (**a**) Rotating speed of the cage; (**b**) Rotating speed of the ball; (**c**) Contact force between ball and inner ring; (**d**) Contact force between ball and outer ring.

According to empirical formula, the bearing cage speed n_c is

$$n_c = \frac{1}{2}[n_i(1-\gamma) + n_o(1+\gamma)] \tag{5}$$

where n_i is the rotating speed of inner rings and n_o is outer rings speed.

$$\gamma = \frac{D_w \cos \alpha}{d_m} \tag{6}$$

where α is ball connect angle.

It is obtained that the cage speed is 430.21 r/min while the simulation value is 432.92 r/min, and the difference is 0.63%, so the simulation results can be considered reasonable.

For ball bearings subjected to combined axial and radial loads, due to the influence of centrifugal force and gyro torque, the indirect contact angle between the rolling element and raceway at different phase angles is different, and the contact load between the rolling element and the inner and outer rings is also different. If the applied radial load is recorded as *Fr*, axial load is *Fa*, and the included angle between adjacent rolling elements is ϕ, the rolling element at ϕ = 0 will bear the maximum load $Q_{\max}$ [32].

The maximum contact load of ball bearings under combined load is:

$$Q_{\max} = \frac{Fr}{ZJ_r(\varepsilon)\cos\alpha} \tag{7}$$

where $J_r(\varepsilon)$ can be obtained by referring to Table 7.4 of the reference [33].

The load distribution function at different phase angles is:

$$Q_{\phi i} = Q_{\max}\left[1 - \frac{1}{2\varepsilon}(1 - \cos\phi)\right]^{1.5} \tag{8}$$

Applying radial and axial forces of 500 N to bearing, the result calculated by empirical formulas is shown in Figure 2.

The bearing static load distribution curve reflects the bearing load distribution in the stationary or ultra-low speed conditions of the bearings. For bearings running at medium and high speeds, collisions are generated between the components during the motion, resulting in instantaneous increase in load values between the rolling element and raceway or cage. Considering that the load curve in dynamic analysis is more confusing, the obtained dynamic load curve needs to be filtered to eliminate the burr of the signal. Static simulation and dynamic simulation were carried out by applying the same load conditions to the bearing model in ADAMS, and the load magnitudes of the rolling element under different phase angles were obtained. Accordingly, the static load distribution curve and dynamic load distribution curve are plotted and the results are shown in Figure 8.

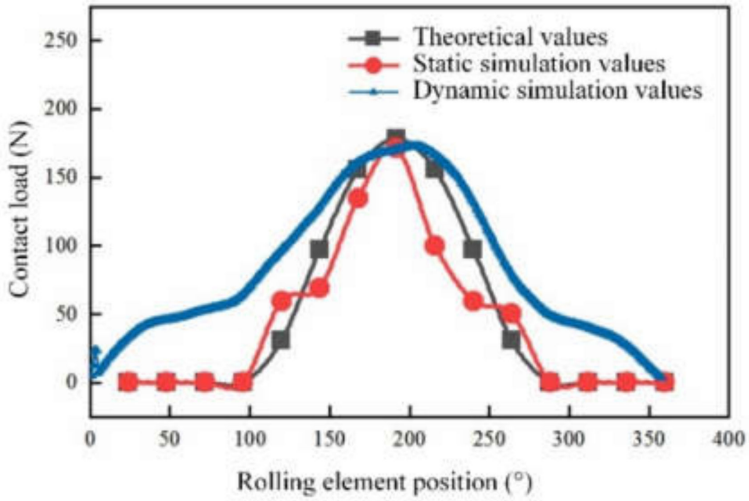

Figure 8. Comparison of dynamic simulated, static simulated and theoretical values of combined load.

According to Figure 8, the dynamic load curve is roughly similar to the static simulation results and the load curve profile obtained from theoretical calculation, which proves that the bearing dynamic model in Section 2 is correct. In the real service process, the dynamic load profile is obviously not as stable as the other two static load profiles, due to the random collision between the rolling element and inner and outer rings, rolling element and cage, cage and inner and outer rings during the bearing motion. Additionally, due to the existence of inertia moment and centrifugal force, the non-load-bearing area where the contact load between rolling body and raceway is 0 under theoretical or static simulation conditions, and the same contact load exists under dynamic simulation conditions. Therefore, it is reasonable that the dynamic load curves are partially different from the static simulation curves in the validation analysis of the dynamics model.

4. Analysis of Dynamic Characteristics of the Cage

The dynamic characteristics of the cage have different performances with the change in working conditions. In previous studies [30,33,34], it is usually judged according to the motion state of the centroid: when the trajectory of the cage centroid is one point, it can be considered as a completely stable state; when the cage centroid trajectory is not a point and a vortex occurs, the motion stability of the cage is judged according to the centroid vortex trajectory and the vortex velocity deviation ratio. When the cage vortex trajectory is almost circular, it indicates that the cage centroid is in a stable vortex state. When the value of the cage vortex velocity deviation ratio is small, it indicates that its motion is relatively stable.

The deviation ratio of cage vortex velocity is expressed as σ_{v}, and the calculation formula is as follows:

$$\sigma_{\mathrm{v}} = \frac{\sqrt{\sum_{i=1}^{n} (v_i - \overline{v}_{\mathrm{m}})^2/(n-1)}}{\overline{v}_{\mathrm{m}}} \tag{9}$$

where v_i is the speed of the cage centroid at any moment, $\overline{v}_{\mathrm{m}}$ is the average speed of the cage centroid, and n is the number of sampling points of the cage speed time domain curve.

4.1. Stability Variation of Cage with Rotating Speed

Apply 1000 N axial load to the bearing, observe the simulation results at driving speeds of 1000, 2000, 3000, 4000, 5000, 6000, 7000 and 8000 r/min, and analyze the influence of speed on the stability of cage.

The trajectory of the cage centroid after stabilization obtained by simulation analysis at the above 8 different rotating speeds is shown in Figure 9.

From Figure 9, it can be seen that the vortex radius is close to the guiding gap after stabilization. When the rotating speed is less than 3000 r/min, the cage centroid trajectory tends to change steadily and regularly with the increase in rotating speed; after exceeding 3000 r/min, the centroid trajectory tends to become cluttered with the increase in rotating speed; after exceeding 6000 r/min, it changes relatively invisibly.

Figure 10 shows the vortex radius ratio and vortex velocity deviation ratio of the cage centroid trajectory. The vortex radius ratio is the ratio of the difference between the maximum and minimum vortex radius to the average vortex radius, and it reflects the divergence degree of the cage centroid vortex trajectory. It can be seen from the figure that the ratio value decreases gradually with the increase in speed when the speed is less than 3000 r/min, when the speed exceeds 3000 r/min, the deviation ratio of centroid vortex velocity increases gradually with the increase in speed, and finally tends to be level off. It is noteworthy that both ratios almost have the same trend, but the vortex radius ratio has a greater magnitude of change. Even so, its range of variation with rotating speed is only 0.15, so the effect of speed on cage stability can be considered small.

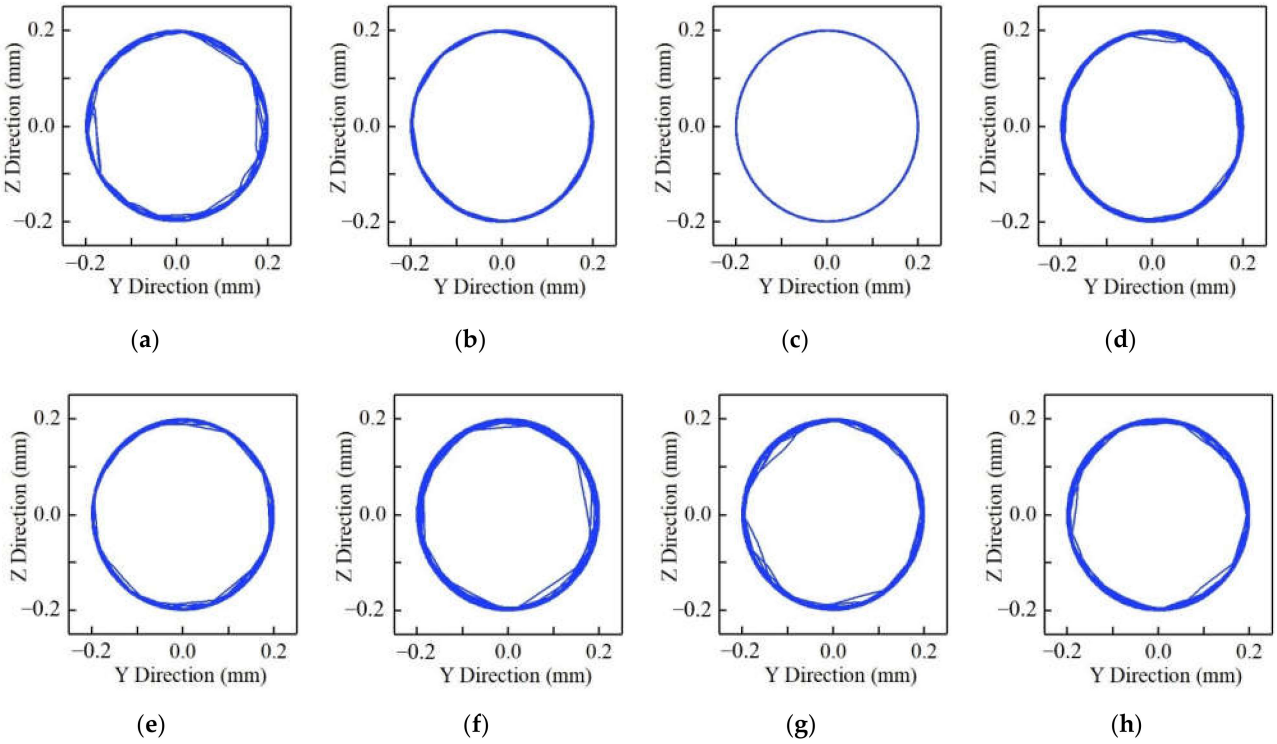

Figure 9. Cage centroid trajectory at different speeds. (**a**) 1000 r/min; (**b**) 2000 r/min; (**c**) 3000 r/min; (**d**) 4000 r/min; (**e**) 5000 r/min; (**f**) 6000 r/min; (**g**) 7000 r/min; (**h**) 8000 r/min.

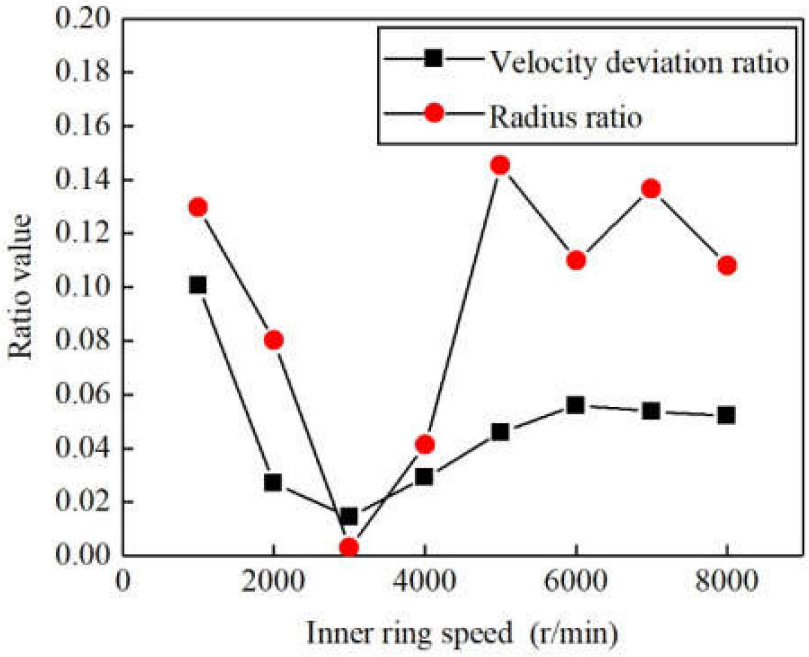

Figure 10. Effect of rotating speed on the velocity deviation ratio and radius ratio of cage centroid vortex velocity.

As can be seen from Figures 9 and 10, the motion stability of the cage gradually stabilizes with an increase in speed and then gradually deteriorates to a certain level. This is due to the fact that with the increase in rotating speed, the unbalanced force of the cage itself and the interaction with the steel ball gradually increase, but the increasing amplitude of the cage unbalanced force is large and plays a major role, prompting the cage to push

towards the guide surface of the guiding ring and produce a stable vortex. When the rotating speed exceeds 3000 r/min, the interaction between the cage pocket and the steel ball increases, gradually changes the motion state of the cage, presents a trend of gradual confusion, and the motion stability becomes worse. Compared with the simulation results of Wen [34], the stability trend of the bearing cage in this paper is in good agreement with the simulation results of the angular contact ball bearing 7103AC, which verifies the correctness of the simulation results.

4.2. Stability Variation of Cage with Pure Axial Load

Apply the driving speed of 1000 r/min to the bearing and select the simulation analysis results of five different working conditions of 1000, 2000, 3000, 4000 and 5000 N to analyze the influence of axial load on the stability of cage. The trajectory of the cage centroid obtained under the action of the above five different axial forces is shown in Figure 11.

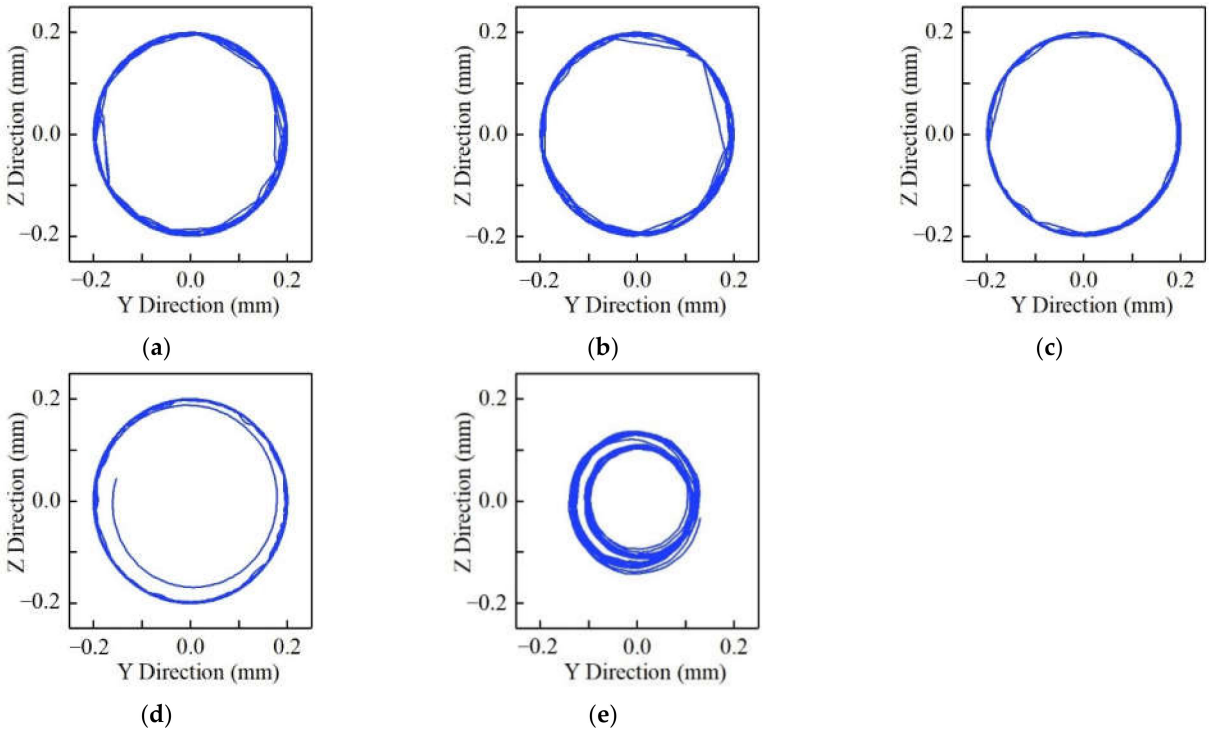

Figure 11. Cage centroid trajectory at different axial load. (**a**) Cage centroid trajectory at 1000 N; (**b**) Cage centroid trajectory at 2000 N; (**c**) Cage centroid trajectory at 3000 N; (**d**) Cage centroid trajectory at 4000 N; (**e**) Cage centroid trajectory at 5000 N.

It can be seen from Figure 11 that when the axial force is less than 3000 N, the trajectory of the cage centroid tends to be stable and regular with the increase in the axial force; after more than 3000 N, the trajectory of the centroid tends to be more complex with the increase in axial load.

The vortex radius ratio and vortex velocity deviation ratio are shown in Figure 12. It can be seen that when the axial force is less than 3000 N, the ratios gradually decrease with the increase in axial force, and when the axial force exceeds 3000 N, they enhance with the increase in axial force. The vortex radius ratio has a variation of 0.45, so the effect of axial force on cage stability is significant.

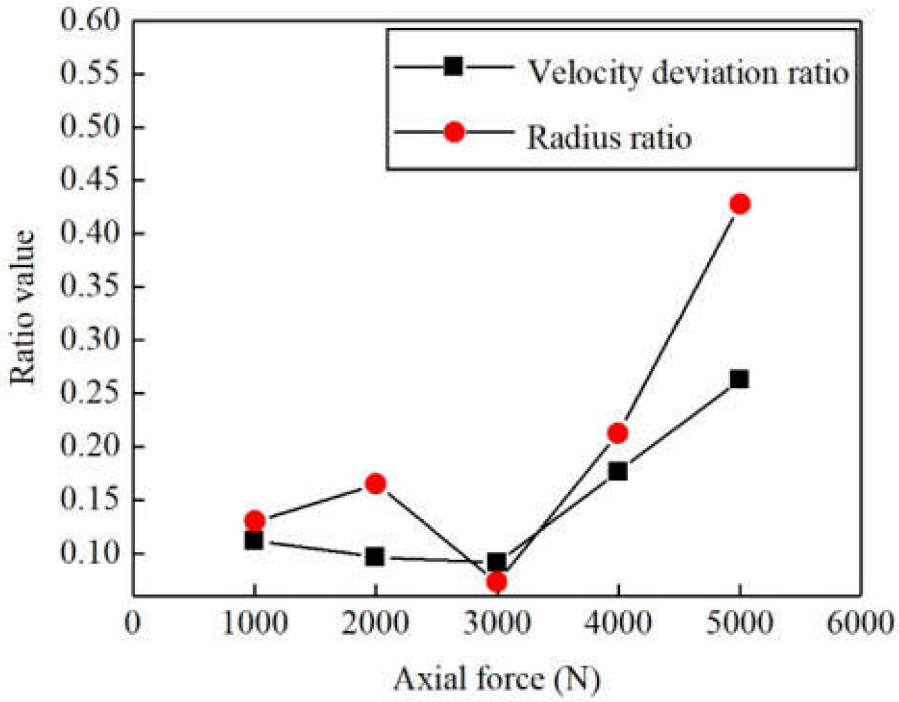

Figure 12. Effect of pure axial load on the velocity deviation ratio and radius ratio of the cage centroid trajectory.

It can be seen from Figures 11 and 12 that within a certain axial force range, the motion stability of the cage tends to be stable with the increase in the axial force. After exceeding the critical value, the stability of the cage gradually deteriorates. This is because within a certain range of axial force, with the increase in axial load, the load borne by each steel ball is gradually uniform. Therefore, the difference in the guiding ring drag force leads to the reduction in the fluctuation of rotating speed when the steel ball rotates to different azimuth angles, which reduces the collision between the steel ball and the cage pocket. The unbalanced force of the cage is dominant, which makes the cage show a stable vortex, which is conducive to the stability of the movement of the bearing cage. When the axial force is too large, the collision force fluctuation between the steel ball and the cage pocket hole increases, making the stability of the cage worse.

4.3. Stability Variation of Cage with Radial Load

FPCBB cannot bear pure radial force, the size of radial force it can bear should be less than 0.7 times of axial force. The simulation analysis results of 6 different radial force working conditions of 100, 200, 300, 400, 500 and 600 N are selected to analyze the influence of radial force on the stability of the cage under the combined load condition. The trajectory of the cage centroid obtained under the above six different working conditions is shown in Figure 13, from which it can be seen that the cage centroid trajectory is gradually complicated with the increase in radial force.

The vortex radius ratio and vortex velocity deviation ratio under the above six different load conditions are shown in Figure 14. It can be seen that the ratios have an upward trend and the trend tend to expand. The amplitude of the radius ratio exceeds 1.0 when the radial force is 600 N. It can be considered that the radial force has the greatest influence on the stability of the cage, and the influence enhances with the increase in the radial force.

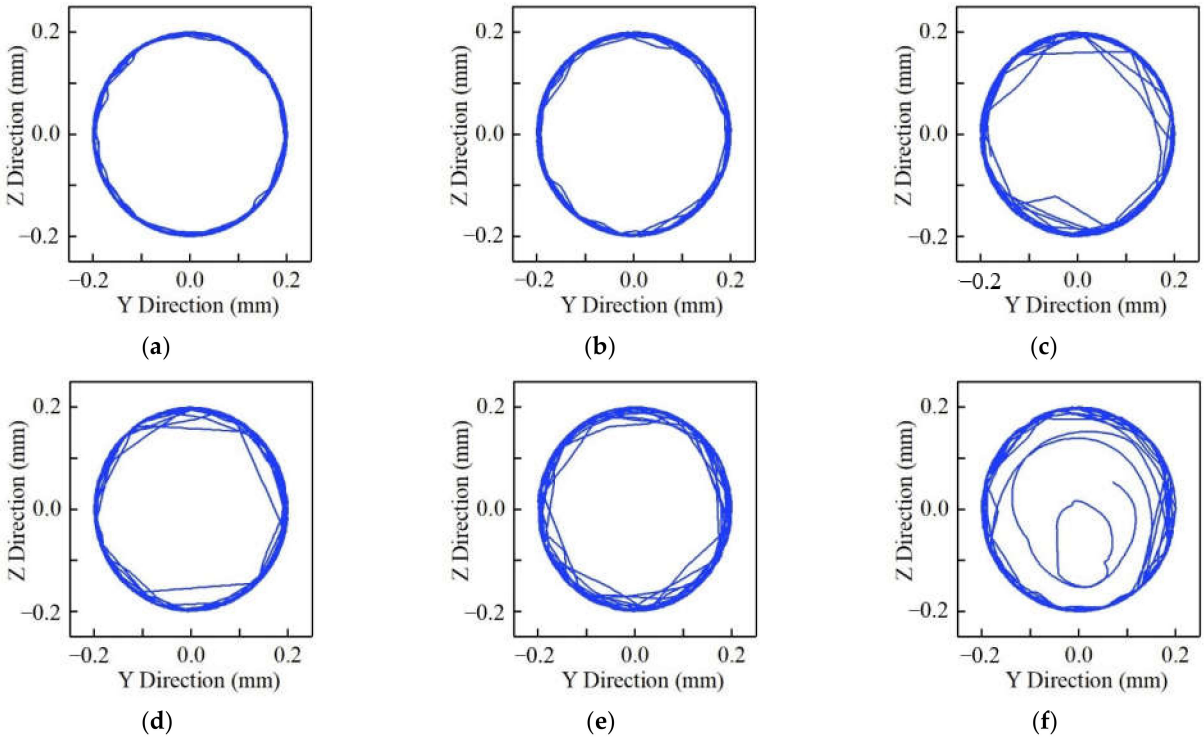

Figure 13. Cage centroid trajectory at different radial load under combined load. (**a**) 100 N; (**b**) 200 N; (**c**) 300 N; (**d**) 400 N; (**e**) 500 N; (**f**) 600 N.

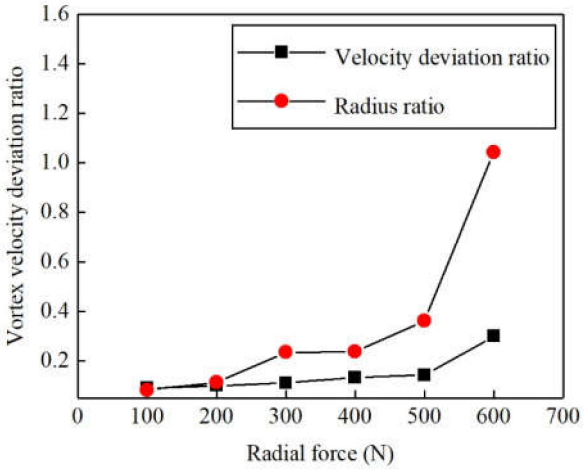

Figure 14. Effect of radial load on the speed deviation ratio and radius ratio of the cage centroid trajectory under combined load.

From Figures 13 and 14, it can be seen that the increase in radial force will prompt the cage centroid motion trajectory tends to be chaotic, and the stability becomes worse. This is because with the increase in radial force, the load of each steel ball is more and more uneven, which increases the frequency and amplitude of the collision between the steel ball and the cage pocket hole, thus changing the cage trajectory, making the trajectory irregular and reducing the stability of the cage.

4.4. Experimental Verification

In order to verify the accuracy of the analysis results of the bearing dynamic model established according to the parametric method in this paper, a rolling bearing cage performance analysis test bed is built. The test bed is composed of motorized spindle, coupling,

support shaft, test shaft, loading device and test system. The main structure is shown in Figure 15. The test bearing is QJ215, its structure is shown in Figure 2. The structural parameters are consistent with the bearing used for simulation.

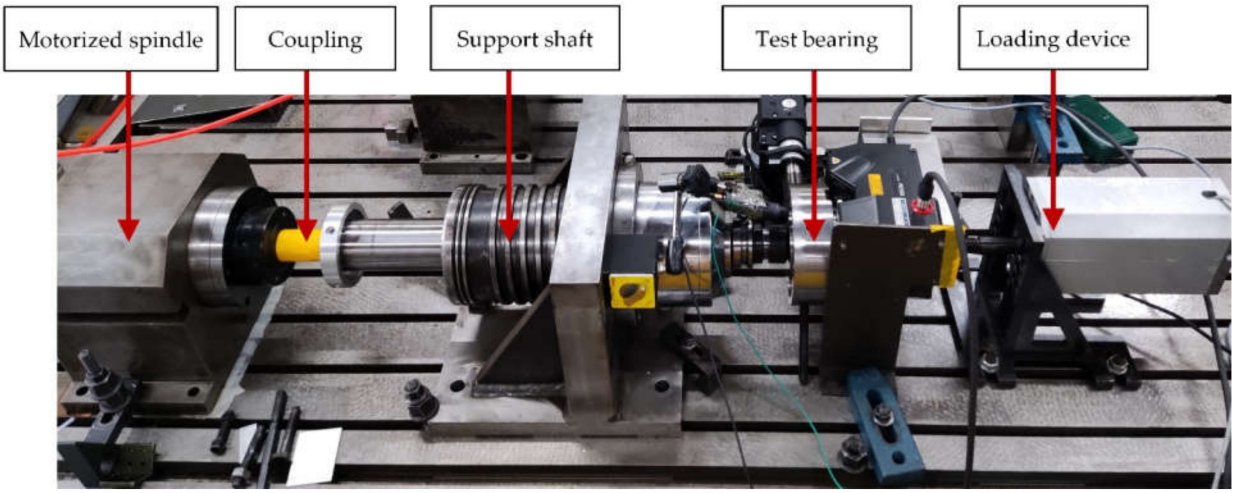

Figure 15. Test bed of rolling bearing cage performance analysis.

The test system includes a rotating speed measurement system and a motion displacement measurement system, as shown in Figure 16. The rotating speed measurement system includes laser speed sensor, reflector, signal acquisition system and computer, etc., and the motion displacement measurement system includes 2D laser profilers and processor.

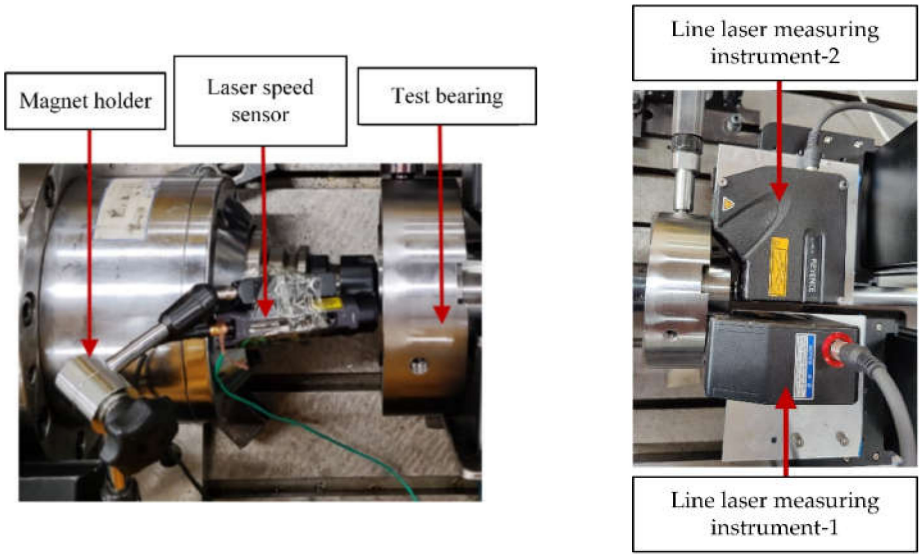

Figure 16. Cage speed and displacement measuring device. (**a**) Cage speed measuring device; (**b**) Cage displacement measuring device.

The principle of cage speed measurement is to put a reflector on the end surface of the cage, and align the laser to the reflector. When the reflector returns to the laser with one revolution of the cage, the laser sensor returns a pulse signal, which is converted into a rotational speed signal by the acquisition system, and finally, the curve of rotating speed of the cage is obtained. The laser sensor is Laser Tacho Probe-MM0360 from Denmark, and the signal acquisition device is PAK Mobile MK II data acquisition system from Millerbem, Germany.

The principle of cage trajectory measurement is shown in Figure 17. The vibration displacement information of the cage is monitored in real time by 2D laser profiler, and the positions of the cage profile edge points at different moments are subtracted to obtain the vibration displacement signal of the cage. Two sensors are used in the test: sensor 1 is placed in the direction parallel to the test bench, for measuring the displacement in the *X*-axis direction; sensor 2 is placed in the direction perpendicular to the test bench, to measure the displacement in the *Z*-axis direction. The two sensors are synchronous and the signal is transmitted to the monitor through a switch. The 2D laser profiler is the LJ-X8020 model from Keyence.

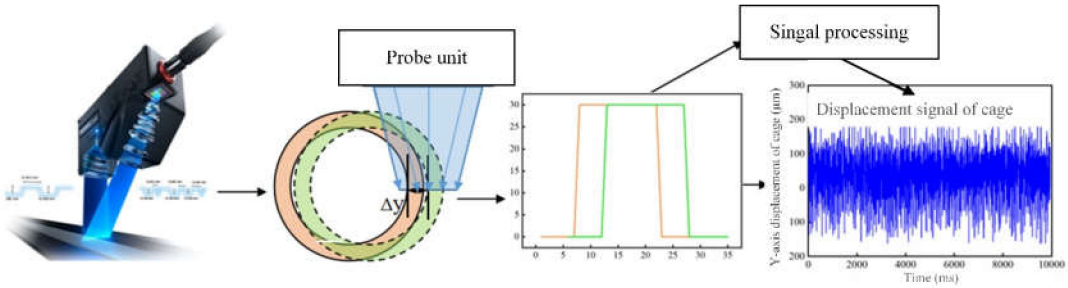

Figure 17. Measurement principle of cage trajectory.

The rotating speed of the cage was measured using the rolling bearing cage motion test bench. The test rotating speed of the electric spindle changes from 600 r/min to 2000 r/min under constant load. The radial force loading device kept 0 N, and the output values of the axial force loading device were from 1000 N to 2000 N. The comparison results between simulation and experiment are shown in Figure 18.

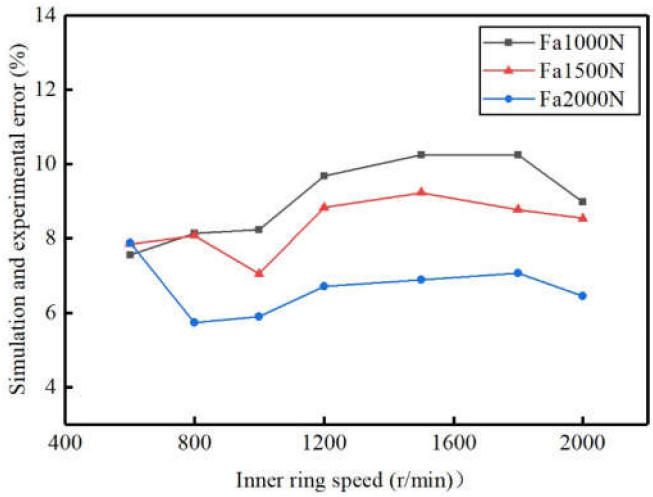

Figure 18. Simulation and experimental error curve.

The experimental speed is higher than the simulated speed, and the maximum error between them is 10.4%. It shows that the rotating speed has little influence on the error, and the error decreases with the increase in the axial load. The main reason for the error is that the test bearing adopts SKF's LGMT 3/1 grease, whose base oil viscosity is 125 mm^2/s. Its typical application is bearings with > 100mm inner diameter. It is larger than the viscosity recommended in the manual of QJ215. Thus, the drag force between the rolling body and the inner and outer rings is larger, which causes the cage speed to increase. Therefore, the simulation results can be considered to be consistent with the experimental results, and the accuracy of the simulation is verified.

The radial vibration signal of the cage is collected at the driving speeds of 1000, 1500 and 1800 r/min, as well as 1000 N pure axial load condition. The collected vibration displacement signals are filtered to eliminate the rotating frequency and external interference,

and the centroid trajectory is obtained by synthesizing the two vibration displacement signals. The synthetic centroid trajectory of the cage is shown in Figure 19.

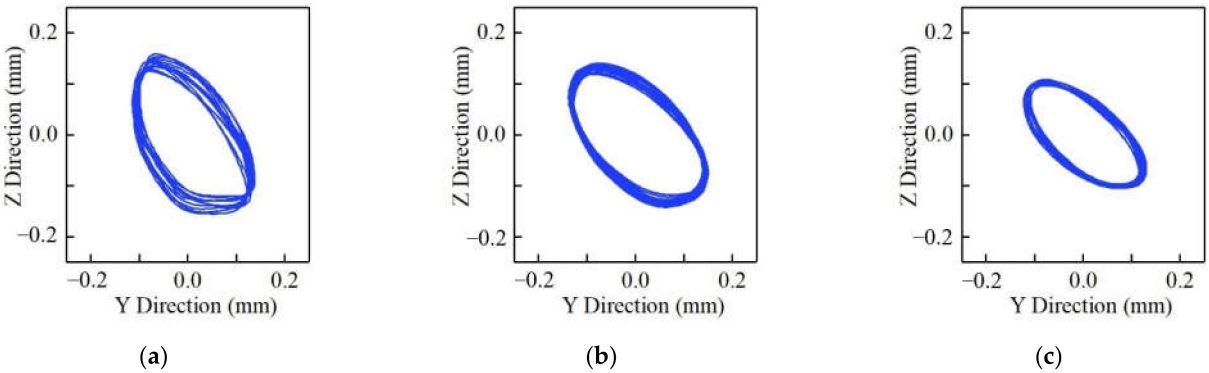

Figure 19. Cage centroid trajectory at different driving speeds. (**a**) 1000 r/min; (**b**) 1500 r/min; (**c**) 1800 r/min.

From Figure 19, it can be found that the centroid trajectory is elliptical, rather than the circle shown in the simulation result of Figure 9, this is caused by the difference in the stiffness of the bearing in all directions due to the actual bearing installation error or the deflection of the loading force. As shown in the figure, in the speed range of 1000–1800 r/min, the centroid trajectory of the cage shows vortex motion and tends to change steadily and regularly with increasing speed. It is consistent with the trend of simulation results of Figure 9.

Similarly, with regard to a change in the operating conditions, the centroid trajectory was analyzed at the speed of 1000 r/min and pure axial loads of 1000, 1500 and 1800 N, respectively, and the results are shown in Figure 15.

It can be seen from the figure that the centroid trajectory with axial force of 1500N and 1800N is better concentrated than that at 1000N, and the cage vortex situation is more stable, which is consistent with the trend of simulation results of Figure 11. From Figures 19 and 20, it can be seen that the change rules of the cage centroid trajectory measured by the experiment is consistent with the change in the simulation results, indicating that the change rules of the centroid trajectory summarized before may be correct, which also verifies the correctness of the simulation. There are still many shortcomings of the experiment. For example, only pure axial force loading is realized. Due to the limitation of conditions, there is no way to stably load radial force and axial force at the same time. High speed makes the test bench vibrate seriously, so for safety and accuracy, only the operation at low speed is simulated.

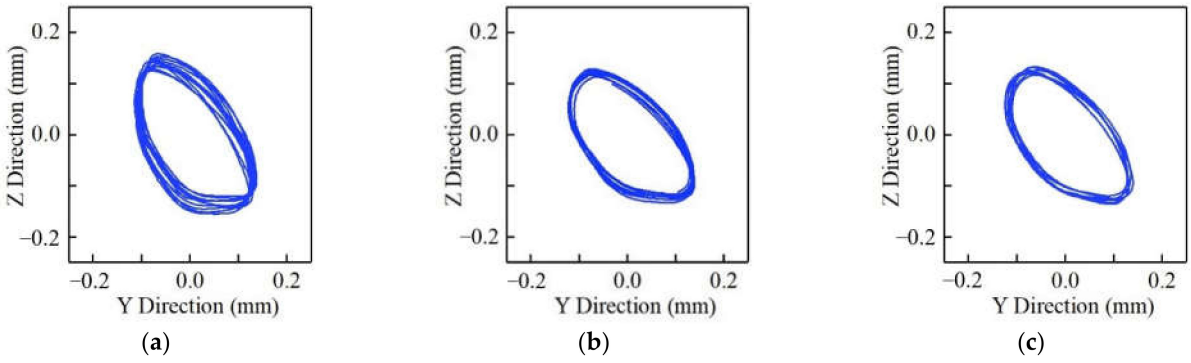

Figure 20. Cage centroid trajectory at different axial forces. (**a**) 1000 N; (**b**) 1500 N; (**c**) 1800 N.

5. Conclusions

In this paper, the dynamic model of FPCBB is established according to the multi-body dynamics simulation software ADAMS and its subroutine GFOSUB, which makes full use of the advantages of ADAMS in solving dynamic equations with high stability. The correctness of the dynamic model is verified by comparing the theoretical calculation results with the static simulation results of the cage speed and bearing load distribution. The effects of rotating speed and load on the stability of the cage are evaluated with the indexes of vortex radius ratio and vortex speed deviation ratio of the cage centroid trajectory. A test bench is established, and measurement methods of the cage speed and centroid vortex trajectory are proposed. The motion stability of cage reflects the stability of bearings; therefore, it is of practical significance to master the operation law of cage and guide the application of four contact point ball bearing. Some conclusions have been given as follows:

The dynamic bearing load curve is similar to the static load curve in overall trend, but the dynamic load curve is less stable than the static load curve, due to the existence of collision force between components.

The cage stability is affected by rotating speed and load conditions. The vortex radius ratio and the vortex velocity decrease and then increase as the inner ring getting faster. When the axial load is small, these two indicators are relatively stable, but after the axial force exceeds 3000 N, the cage becomes more and more unstable. Under both axial load and radial load, the increased radial force reduces cage stability.

The experimental results verify the rationality of the simulation results to a certain extent. It also verifies the feasibility of the speed and centroid vortex trajectory measurement method proposed in this paper. For different four-point contact ball bearings, further simulation and experiments are needed to verify the conclusions of this paper.

Author Contributions: Conceptualization, Y.Z. and J.H.; methodology, Y.L., S.M. and Y.Z.; software, S.M. and G.H.; validation, W.L.; formal analysis, G.H.; funding acquisition, J.H.; data curation, W.L., Y.L. and G.H.; writing—original draft preparation, Y.L. and Y.Z.; writing—review and editing, Y.L. All authors have read and agreed to the published version of the manuscript.

Funding: This research received was funded by the National Science Foundation of China (52175250).

Institutional Review Board Statement: Not applicable.

Informed Consent Statement: Not applicable.

Data Availability Statement: Not applicable.

Acknowledgments: The authors would like to thank the National Science Foundation of China (52175250) for the financial support.

Conflicts of Interest: The authors declare no conflict of interest.

References

1. Tang, W.C.; Chen, G.D.; Sun, Y.C.; Xu, L. Dynamic research and fault simulation on high-speed railway axle box bearings based on ANSYS/LS-DYNA. *Mod. Mach.* **2015**, *5*, 5–10.
2. Lundberg, G.; Palmgren, A. *Dynamic Capacity of Rolling Bearing*; Acta Polytechnica Mechanical Engineering Series; Royal Swedish Academy of Engineering Sciences: Stockholm, Sweden, 1947.
3. Zhang, L.Y.; Wang, Y.S.; Yuan, Q.Q.; Ji, Y.G. Influence of load and geometric parameters on load distribution of single-row four-point contact ball slewing bearings. *J. Mech. Transm.* **2013**, *37*, 27–29.
4. Li, Y.F.; Wu, Z.Y.; Lu, B.H.; Zhao, G.Y.; Sun, L.M. Influence of clearance on load distribution of single row four-point contact ball slewing bearing. *J. Mech. Transm.* **2010**, *34*, 56–58.
5. Li, K.Y.; Tang, W.C. Load-displacement relationship model and measurement of deep groove ball bearing and 4-point contact ball bearing. *J. Mech. Sci. Technol.* **2021**, *35*, 3045–3058. [CrossRef]
6. Wu, L. *Multi-Body Dynamics Analysis of Rigid-Flexible Coupling of Thin-Walled Four-Point Contact Ball Bearings*; Kunming University of Science and Technology: Kunming, China, 2017.
7. Shi, P.F. *Performance Analysis of Thin-Wall Four-Point Contact Ball Turntable Bearings*; Henan University of Science and Technology: Henan, China, 2013.

8. Yang, B.; Yao, T.Q. Finite element analysis of contact characteristics of thin-walled four-point contact ball bearing. *Softw. Guide* **2019**, *19*, 70–73.
9. Liu, Z.M.; Yao, T.Q.; Zhang, Y.W.; Cheng, X. Influence of the structural parameters of thin-wall four-point contact ball bearings on the mechanical. *J. Mach. Des.* **2021**, *38*, 7–13.
10. Walters, C.T. The Dynamics of Ball Bearings. *J. Lubr. Technol.* **1971**, *93*, 1–10. [CrossRef]
11. Gupta, P.K. *Advanced Dynamics of Rolling Elements*; Springer: New York, NY, USA, 1984.
12. Gupta, P. Modeling of Instabilities Induced by Cage Clearances in Cylindrical Roller Bearings. *ASLE Trans.* **1991**, *34*, 1–8. [CrossRef]
13. Gupta, P. Some Dynamic Effects in High-Speed Solid-Lubricated Ball Bearings. *ASLE Trans.* **1983**, *23*, 393–400. [CrossRef]
14. Hagiu, G.D.; Gafitanu, M.D. Dynamic characteristics of high speed angular contact ball bearings. *Wear* **1997**, *211*, 22–29. [CrossRef]
15. Wijnant, Y.H.; Vensing, J.A.; Nijen, G.C. The influence of lubrication on the dynamic behavior of ball bearings. *J. Sound Vib.* **1999**, *222*, 579–596. [CrossRef]
16. Weinzapel, N.; Sadeghi, F. A discrete element approach for modeling cage flexibility in ball bearing dynamics simulations. *J. Tribol.* **2009**, *131*, 110–119.
17. Daidié, A.; Chaib, Z.; Ghosn, A. 3D Simplified Finite Elements Analysis of Load and Contact Angle in a Slewing Ball Bearing. *Mech. Des.* **2008**, *130*, 082601. [CrossRef]
18. Iker, H.; Josu, A.; Mikel, A.; Ibai, C.; Iñigo, E. Load distribution and friction torque in four-point contact slewing bearings considering manufacturing errors and ring flexibility. *Mech. Mach. Theory* **2019**, *137*, 23–36.
19. Josu, A.; Mikel, A.; Rafael, A.; Igor, F.B. General static load-carrying capacity for the design and selection of four contact point slewing bearings: Finite element calculations and theoretical model validation. *Finite Elem. Anal. Des.* **2012**, *55*, 23–30.
20. Ammarullah, M.I.; Afif, I.Y.; Maula, M.I.; Winarni, T.I.; Tauviqirrahman, M.; Akbar, I.; Basri, H.; Heide, E.; Jamari, J. Tresca Stress Simulation of Metal-on-Metal Total Hip Arthroplasty during Normal Walking Activity. *Materials* **2021**, *14*, 7554. [CrossRef]
21. Ji, B.W.; Jing, M.Q.; Liu, Q. Dynamic Analysis and Simulation of Ball Bearing Cage Based on ADAMS. *Mach. Build. Autom.* **2014**, *43*, 113–116.
22. Hong, J.C.; Zhang, T.Z.; Cui, B.R.; Fu, C.X. *Parametric Modeling and Dynamic Simulation of Rolling Bearing Based on ADAM*; Qingdao University: Qingdao, China, 2014.
23. Chan, W.B.; Yao, T.Q. Multi-body Dynamics Analysis of Angular Contact Ball Bearings. *New Technol. New Process* **2014**, *2*, 46–49.
24. Hou, Y.; Xiong, X.Y.; Wang, X.; Niu, X.M. Dynamic co-simulation based on ANSYS and ADAMS and its application. *Min. Process. Equip.* **2014**, *42*, 111–115.
25. Zhang, Y.W.; Yao, T.Q.; Liu, Z.M.; Cheng, X. Stability Study of Thin-Walled Four-Point Contact Ball Bearing Cage. *Light Ind. Mach.* **2021**, *39*, 1–6.
26. Zhao, J.; Yao, T.Q.; Chen, R.B. Dynamics Simulation Analysis of Single Row Four Point Contact Ball Slewing Bearing. *J. Mech. Transm.* **2020**, *44*, 130–136.
27. Li, C. *ADAMS/View Parametric Design Technology and the Application in Mechanical Engineering*, 1st ed.; Science Press: Beijing, China, 2018; pp. 111–116.
28. Ma, S.J.; Zhang, X.; Yan, K.; Zhu, Y.S.; Hong, J. A Study on Bearing Dynamic Features under the Condition of Multiball–Cage Collision. *Lubricants* **2022**, *10*, 9. [CrossRef]
29. Deng, S.E.; Jia, Q.Y. *Roller Bearing Design Principle*, 2nd ed.; Standards Press of China: Beijing, China, 2008; pp. 85–87.
30. Ye, Z.H. *Research on Dynamic Behavior of High Speed Rolling Bearing in Aeroengines*; Harbin Institute of Technology: Harbin, China, 2013.
31. Yao, T.Q.; Wang, L.H.; Liu, X.B.; Huang, Y.Y. Multibody dynamics simulation of thin-walled four-point contact ball bearing with interactions of balls, ring raceways and crown-type cage. *Multibody Syst. Dyn.* **2020**, *48*, 337–372. [CrossRef]
32. Lu, Q. *Dynamic Analysis and Structural Optimization of the Angular Contact Ball Bearing on ADAMS*; Guangdong University of Technology: Guangdong, China, 2016.
33. Liu, X.H. *High-Speed Rolling Bearing Dynamics Analysis Model and Cage Dynamic Performance Research*; Dalian University of Technology: Dalian, China, 2011.
34. Wen, B.G. *Dynamic Characteristics of Angular Contact Ball Bearing Cage and Experimental Study*; Dalian University of Technology: Dalian, China, 2017.